

Emergent explosive synchronization in adaptive complex networks

Vanesa Avalos-Gaytán

Research Center in Applied Mathematics, Univ. Autónoma de Coahuila, Saltillo, Coahuila, Mexico

Juan A. Almendral and I. Leyva

*Center for Biomedical Technology, Univ. Politécnica de Madrid, 28223 Pozuelo de Alarcón, Madrid, Spain and
Complex Systems Group & GISC, Univ. Rey Juan Carlos, 28933 Móstoles, Madrid, Spain*

F. Battiston, V. Nicosia, and V. Latora

School of Mathematical Sciences, Queen Mary University of London, London E1 4NS, United Kingdom

S. Boccaletti

*CNR-Institute of Complex Systems, Via Madonna del Piano, 10, 50019 Sesto Fiorentino, Florence, Italy and
Embassy of Italy in Israel, Trade Tower, 25 Hamered St., 68125 Tel Aviv, Israel*

Adaptation plays a fundamental role in shaping the structure of a complex network and improving its functional fitting. Even when increasing the level of synchronization in a biological system is considered as the main driving force for adaptation, there is evidence of negative effects induced by excessive synchronization. This indicates that coherence alone can not be enough to explain all the structural features observed in many real-world networks. In this work, we propose an adaptive network model where the dynamical evolution of the node states towards synchronization is coupled with an evolution of the link weights based on an anti-Hebbian adaptive rule, which accounts for the presence of inhibitory effects in the system. We found that the emergent networks spontaneously develop the structural conditions to sustain explosive synchronization. Our results can enlighten the shaping mechanisms at the heart of the structural and dynamical organization of some relevant biological systems, namely brain networks, for which the emergence of explosive synchronization has been observed.

I. INTRODUCTION

Adaptivity is a key feature in the construction and function of many real complex systems. In the brain, for instance plasticity is at the heart of memory and learning processes, and governs the huge functional versatility of this system. In many modeling approaches, synchronization has been studied as the emerging collective phenomenon of interest in a population of interacting dynamical units, and the target of adaptation has been considered to be the improvement of the level of synchronization in the system [1, 2]. Most of the works in this area have implemented different versions of the Hebbian adaptation rule as a generative mechanism to enhance the strengths of the links of a network [3–5]. As a result, the origin of various emerging features of real-world networks, such as scale-free topologies [6], modularity [3, 4], or assortativity [5], has been better understood.

However, even if brain synchronization, both at the scale of neurons and at that of cortical areas, has proved to be fundamental for the proper functioning of the brain, improving the coherence cannot be the only mechanism at work in brain networks. In fact, it is well known that oversynchronization can destroy the overall complexity of the system, reducing the amount of information that the system is able to process and eventually leading to pathological states as epilepsy [7]. For this reason, inhibition and anti-Hebbian coupling have been investigated in neural systems, and they have been shown to play an important role in the control of excessive synchronization

and redundancy [8–10], and also in the context of circadian rhythms [11]. Anti-Hebbian rules have also been considered more in general in adaptive complex networks, and it has been found that they can be useful to generate features as criticality [12], dissasortativity [6], structural heterogeneity [13], bistability [14] or multistability [15].

In this work, we introduce and study an adaptive complex network model in which the nodes are coupled oscillators trying to synchronize their phases, while the link weights evolve with an anti-Hebbian rule which weakens the connection between pairs of coherent nodes. We will show that the competition between the attractive coupling and the anti-Hebbian link dynamics generates networks with interesting topological and dynamical features. In particular, we find that the networks produced by our model are able to sustain explosive synchronization (ES), and this happens for large range of the two tuning parameters of the model. Explosive synchronization, i.e. the sudden, discontinuous and irreversible transition from an incoherent state to a fully synchronized one, is a phenomenon that has attracted special attention in last few years [16–21]. Explosive synchronization has been also observed experimentally in power grids [22], circuits [23] and chemical reactions [24]. More recently, the interest has extended also to neuroscience, and some experimental studies have related explosive synchronization to the onset of seizures [25], and the transition to and from consciousness in anaesthetized patients [26, 27]. Our results indicate that the frustration induced by an anti-Hebbian adaptation rule that promotes links between

nodes in anti-phase dynamics, can be the main responsible of the phenomena observed empirically in neuroscience. Thus, having a simple model that produces networks able to suddenly switch to full coherence, can turn very useful to explore the role of the different tuning parameters and to understand the basic mechanisms behind explosive synchronization in neural systems.

The article is organized in the following way. In Section II we introduce our new coevolving network model coupling node synchronisation and anti-Hebbian pairwise interactions. In Section III we show by mean of numerical simulations the basic structural and dynamical feature of the emerging networks, and how they sustain explosive synchronization. In Section IV we consider the simplified version of the model with only two coupled oscillators, which is amenable to analytical solution and allows to grasp the basic mechanisms at work in the considered coevolving process also for larger coupled systems. Finally we draw our conclusions in Section V.

II. THE MODEL

We consider a system of $N = 300$ all-to-all coupled Kuramoto oscillators, the simplest and most common way to describe synchrony in nature [28, 29]. Each oscillator is characterized by its phase θ_l , with $l = 1, \dots, N$, whose dynamics is ruled by the equations:

$$\dot{\theta}_l = \omega_l + \frac{\sigma_c}{N} \sum_{m=1}^N \alpha_{lm} \sin(\theta_m - \theta_l), \quad (1)$$

where ω_l is the natural frequency associated to the oscillator, that is assigned randomly from a uniform distribution in the interval $[0.8, 1.2]$, $\alpha_{lm} \in [0, 1]$ is the weight of the connection between the units l and m , and σ_c is the so-called *coupling strength*, the control parameter that allows to tune the strength of the interactions. Despite the original model was not devised to describe neurons or groups of neurons, in its simplicity, the model is able to capture the gist of a synchronous behavior, which explains why it is nevertheless useful for the investigation of brain networks [30, 31]. In our work we consider the case in which the weight of a link can differ from one pair of nodes to another. Furthermore, we assume that the weights of the links can change in time according to the dynamics of the corresponding two end nodes. Namely, the quantities α_{lm} , with $l, m = 1, \dots, N$, are considered to be time dependent variables, $\alpha_{lm} = \alpha_{lm}(t)$, obeying a differential logistic equation, with a growth rate which depends on the correlations of the two corresponding oscillators l and m . The equations read:

$$\dot{\alpha}_{lm} = (p_c - p_{lm}) \alpha_{lm}(1 - \alpha_{lm}), \quad (2)$$

where $p_{lm} = p_{lm}(t)$ is the instantaneous phase correlation between units l and m at time t , defined as:

$$p_{lm}(t) = \frac{1}{2} \left| e^{i\theta_l(t)} + e^{i\theta_m(t)} \right|, \quad (3)$$

and p_c is a *correlation threshold*. The threshold is the second tuning parameter of our model, and has the following meaning. Whenever $p_{lm}(t) < p_c$, the weight of the link (l, m) gets increased by the dynamical evolution of Eq. (2), while the weight α_{lm} is decreased when $p_{lm}(t) > p_c$. Thus, once the value of p_c is fixed, the links connecting pairs of oscillators with a higher (lower) level of instantaneous synchronization will be weakened (reinforced). As we will show, such a mechanism of frustration of the local synchronization process, which affects a larger number of pairs the higher is the value of p_c , is an essential ingredient for the emergence of explosive synchronization. Notice that Eq. (2) is bistable, and therefore each weight $\alpha_{lm}(t)$ will tend to converge in time to either one of the two values, 0 or 1. As a consequence, for any given choice of the two tuning parameters of our model, σ_c and p_c , and a random sampling of the initial conditions $\theta_l(t=0) = \theta_l(0)$, and $\alpha_{lm}(t=0) = \alpha_{lm}(0)$, the coevolution of oscillator states and link weights governed by Eq. (1) and Eq. (2) will result in a progressive pruning of the links of the initially complete graph, until the system reaches an asymptotic state, defined by $\dot{\alpha}_{lm} = 0, \forall l, m$, corresponding to a specific dynamically-induced network topology.

The phase correlation introduced in Eq. (3) is an instantaneous measure of the correlations between two nodes, and it does not depend on any long-term synchronization process [5]. This represents a qualitative difference between the present study and that conducted in Refs. [3, 4], where it was shown that memory dependent adaptation mechanisms may induce the simultaneous appearance of synchronized clusters and scale-free distributions for the weights of a network. Here, instead, is the adaptive nature of the interactions that directly shapes the topology of a network, and all what will be discussed hereinafter will be about the connectivity properties of the emergent network structure.

III. RESULTS

For a large range of parameters σ_c and p_c we measure the final degree of global synchronization by means of the Kuramoto order parameter

$$R := \left\langle \frac{1}{N} \left| \sum_{l=1}^N e^{i\theta_l(t)} \right| \right\rangle_t,$$

with $R \approx 1$ indicating a fully synchronized graph, and $R \approx 0$ an asynchronous behavior. All the measures are averaged over 10 different instances of the system.

In Fig. 1(a) we characterize the asymptotic dynamics of the network by reporting the average value of R as a function of p_c for different values of σ_c . As expected, for small values of the coupling σ_c the network is not able to synchronize for any value of p_c . However, above the critical coupling for the Kuramoto model $\sigma_c^* = \frac{2}{\pi g(0)} = 0.8/\pi \simeq 0.255$ [32], the global synchronization shows an abrupt transition at $p_c \simeq 0.625$. For

slightly smaller values of σ_c , the global strength suffers also a sharp transition, as shown in Fig. 1(b), pointing out to the fact that the networks go through a phase of strong local synchronization before global coherence is achieved. To better characterize the properties of the

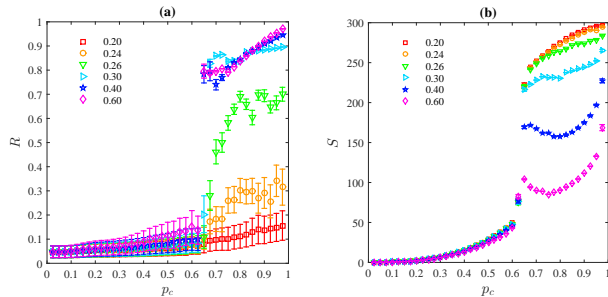


FIG. 1. Asymptotic values of (a) global synchronization, R , and (b) total strength, S , in coevolving weighted networks governed by Eqs. (1) and (2), as a function of the correlation threshold p_c , and for different values of the coupling strength σ_c . When $\sigma_c > \sigma_c^* \simeq 0.255$, abrupt transitions indicating the emergence of explosive synchronization are observed at $p_c \simeq 0.625$.

emerging networks, in the following we analyse the adjacency matrices $A = \{a_{lm}\}$ associated to the original weighted graphs $W = \{\alpha_{lm}\}$, where we set $a_{lm} = 1$ if $\alpha_{lm} > \tau$, and $a_{lm} = 0$ otherwise. We choose $\tau = 0.8$ as a very conservative threshold to ensure that we keep all the significant links. The system is explored for $p_c = [0.6, 1]$ and $\sigma_c = [0.2, 1]$, the relevant parameter range deduced from Fig. 1. As the thresholding process can lead to node pruning, we have performed a component analysis and computed the size N_G of the largest connected component. Results are again averaged over 10 different realization of the process. Fig. 2(a) shows a heat map of the average size of the giant connected component $N_G(\sigma_c, p_c)$ for each pair of control parameters (σ_c, p_c) . We notice that in a large area of the phase diagram, all the $N = 300$ nodes belong to a single component. However, when measuring the average degree $\langle k \rangle$ in Fig. 2(b), we observe that the network connectivity decreases from that of fully connected networks to $\langle k \rangle = 2$ for large values of σ_c .

A more interesting information is retrieved when the correlations between the microscopic features are inspected. In Fig. 3 we show for three representative values of p_c , namely 0.62 (left), 0.87 (center) and 0.97 (right panels), for a fixed value $\sigma_c = 0.6$ -high enough to enable synchronization as shows Fig. 1(a)-, how the emergent network structure and its dynamics are intertwined. In the first row of Fig. 3 the degree of each node k_l is pictured as a function of the frequency ω_l . Before the transition ($p_c = 0.62$), the two features are uncorrelated. However, after the transition, a strong correlation between k_l and ω_l appears, meaning that the nodes with ω_l at the two edges of the natural frequency distribution are much more connected. This is a surprising and noticeable fea-

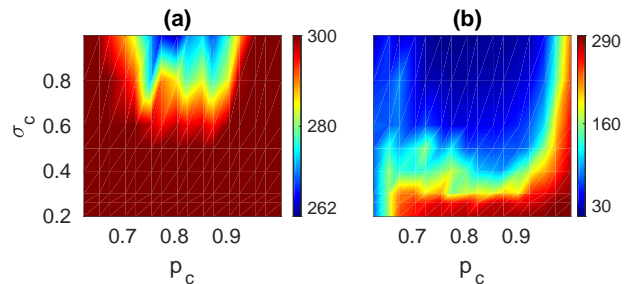


FIG. 2. (a) Size of the giant connected component, N_G , in the asymptotic binarized networks and (b) average degree $\langle k \rangle$, as a function of the coupling strength σ_c and of the correlation threshold p_c .

ture, as V-shape k - ω relationships are well known to be characteristic of networks capable of sustaining explosive synchronization [17–20]. The finding is confirmed by the fact that the dynamics in Eq. (2) forces the network to acquire *frequency dissortativity*, i.e., nodes are much more likely to link to those with distant frequencies, as can be seen in the central row of Fig. 3, where we plot the frequency detuning of each node with its averaged neighbor frequency $\omega_l - \langle \omega_m \rangle_l$, where $m \in \mathcal{G}_l$ are the nodes in the neighborhood of node l . The phenomenon is especially striking just after the transition (center panel). In addition, we also see that for intermediate values of p_c , the detuning is bistable inside the same network.

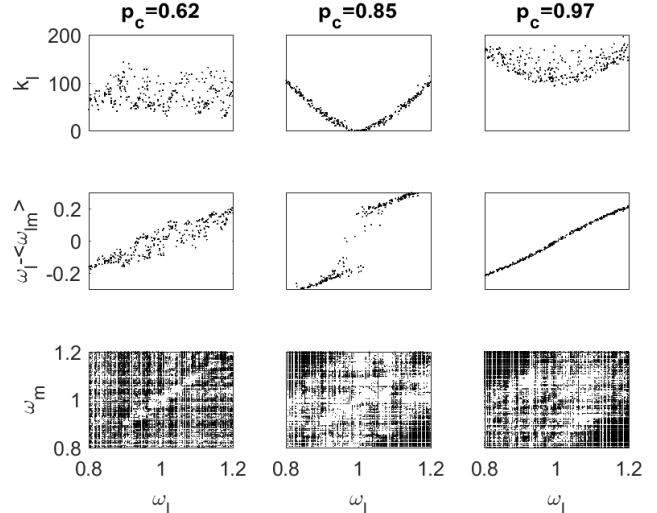


FIG. 3. Scatter plot of the node degree k_i (upper row panels) and of the node neighborhood detuning $\omega_i - \langle \omega_{im} \rangle$ (central row panels) as a function of the natural frequency ω_i of a node for $\sigma_c = 0.6$. The connectivity of the resulting networks are shown as matrices where nodes are placed according to their natural frequencies ω (bottom row panels).

These results show that the link evolution has actually reinforced links connecting nodes whose frequencies are as far as possible, progressively pruning the remaining

connections. This process can be followed through the panels in the bottom row of Fig. 3, where the full connectivity matrix is plotted as a function of (ω_l, ω_m) . Before the transition to synchrony (first column, $p_c=0.62$) the pruning affects only nodes with frequencies close to the center of the distribution, as can be seen in the left panel. As p_c grows, the link suppression affects a large number of links connecting nodes with higher detuning and therefore $\langle k \rangle$ and eventually $N_g(\sigma_c, p_c)$ decrease. A further increase of p_c generates larger values of the mean strength in the network, Fig. 1(b), and a slight increase in the number of links above the threshold, as shown in Fig. 3 (right bottom panel).

The structural inspection of the networks obtained through the adaptive process described by Eqs. (1) and (2) has revealed that for a wide range of the tuning parameters the emerging systems present a strong frequency-degree correlation and frequency disassortativity. This hints that such networks could be able to sustain first-order synchronization, here critically controlled by the correlation threshold p_c .

We numerically check this prediction by using the resulting networks as the fixed connectivity support of a system of interacting Kuramoto oscillators, described by the following dynamical equation

$$\dot{\theta}_l = \omega_l + \frac{\sigma}{N(\sigma_c, p_c)} \sum_{m=1}^{N(\sigma_c, p_c)} a_{lm} \sin(\theta_m - \theta_l), \quad (4)$$

where $l = 1, \dots, N(\sigma_c, p_c)$, being $N(\sigma_c, p_c) \leq N$ the size of the binarized network obtained after the adaptive process for parameters (σ_c, p_c) , and $A' = \{a_{lm}\}$ the adjacency matrix of the corresponding largest giant component of size N_g . The coupling strength σ is now set to be the only control parameter, regardless of the original value of σ_c used to create A' . The original frequency ω_l of each node l is maintained to preserve the structure-dynamics correlations which appeared as a result of the adaptive process. The coherence R is monitored as a function of σ by gradually increasing its value along the simulation without resetting the system. As long as we are looking for a possible first-order phase transition, and the expected corresponding synchronization hysteresis, we perform the simulations also in the reverse way: i.e. we start from a given value σ_{max} where the system is found to be synchronized, and gradually decreasing the coupling. In the following, the two sets of numerical trials are termed as *forward* and *backward* branches, respectively, as used in the literature [16, 20].

In Fig. 4(a) we show the synchronization schemes for the same examples whose structures have been studied in Fig. 3 ($\sigma_c = 0.6$; $p_c = 0.62, 0.85, 0.97$). The three types of structures correspond indeed to different dynamical behaviors. For networks obtained with p_c below the transition, where structural-dynamics correlations are not observed, the network synchronizes in a second order, reversible transition (red circles). For p_c values beyond the critical value, the coherence is reached

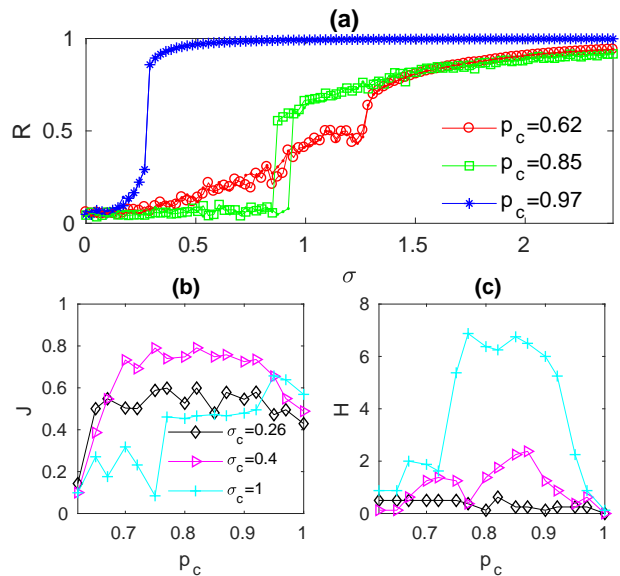


FIG. 4. (a) Global synchronization R for forward and backward synchronization schemes for the binary networks considered in Fig. 3. In panel (b-c) we investigate the abrupt nature of the synchronization transition by reporting the maximum synchronization jump J (b) and the width of the hysteresis loop H (c) as a function of the coupling strength σ_c and of the correlation threshold p_c .

through a first order transition, as suggested by the strong frequency-degree correlations. For intermediate values (green squares), this transition to synchrony is very delayed, and presents an hysteresis loop as a consequence of the bi-stability generated in the detuning distribution (already commented in Fig. 3, central panel). For even larger p_c values (blue diamonds), corresponding to networks with softer k - ω correlation and without gap bi-stability, the synchronization occurs abruptly but reversibly.

A wider overview of how the tuning parameters σ_c and p_c) determine these dynamical behaviors is shown in Fig. 4(b-c). As a measure of abruptness of the synchronization transition, in Fig. 4(b) we compute the average value of the maximum difference in the value of R for two consecutive values of the coupling parameter

$$J := \max_{\sigma} \{R(\sigma + \delta\sigma) - R(\sigma)\}$$

for the forward transition. Similar results are found for the backward transition. In Fig. 4(c), we measure the width of the hysteresis loop by computing the distance between the critical synchronization couplings for the backwards (σ_b) and the forward (σ_f) processes,

$$H := \sigma_b - \sigma_f.$$

As can be seen, the parameter region where the width of the hysteresis loop presents significant values closely corresponds to the values where $N_g(\sigma_c, p_c) < N$, Fig. 2(a), when the frustration for the nodes with frequencies close

to the center of the distribution is so strong that they eventually become disconnected and are removed from the binary network.

IV. ANALYTICAL ANALYSIS OF A SIMPLE ADAPTIVE SYSTEM

To better understand the dynamical system considered in the previous sections, we proceed to analytically study of two oscillators θ_1 and θ_2 coupled by a single weighted link, $\alpha = \alpha_{12} = \alpha_{21}$. For this simplified system, Eqs. (1) and (2) reduce to

$$\begin{aligned}\dot{\theta}_1 &= \omega_1 + \frac{\sigma_c}{2} \alpha \sin(\theta_2 - \theta_1), \\ \dot{\theta}_2 &= \omega_2 + \frac{\sigma_c}{2} \alpha \sin(\theta_1 - \theta_2), \\ \dot{\alpha} &= (p_c - p) \alpha(1 - \alpha),\end{aligned}$$

where $p = p_{12} = p_{21}$ is the instantaneous phase correlation between oscillators 1 and 2 defined in Eq. (3),

$$p = \sqrt{\frac{1 + \cos(\theta_1 - \theta_2)}{2}}.$$

Without loss of generality, we suppose that $\Delta := \omega_1 - \omega_2 > 0$ in order to transform the former set of equations into a two dimensional system with variables α and the phase difference between oscillators $\phi := \theta_1 - \theta_2$, so that we have

$$\begin{aligned}\dot{\phi} &= \Delta - \sigma_c \alpha \sin \phi, \\ \dot{\alpha} &= \left(p_c - \sqrt{\frac{1 + \cos \phi}{2}} \right) \alpha(1 - \alpha),\end{aligned}\quad (5)$$

As it is not possible to integrate Eqs. (5) explicitly, we analyse the system stability to grasp insights on its qualitative behavior. The details of this calculation can be found in the Appendix. We summarize all the results in Fig. 5, which depicts the dynamical behaviors for a system described by Eqs. (5) as a function of the usual coupling strength σ_c and the correlation threshold p_c . The color map of Fig. 5 represents the asymptotic value of the weighted link, as calculated in the Appendix.

Regions $A_{1,2}$ correspond to those parameters for which there is no phase locking: A_1 is defined by $p_c < 1/\sqrt{2}$, and A_2 by $p_c > 1/\sqrt{2}$ and $\sigma_c < \Delta$. The main difference between these two regions is that whereas in A_1 the weight tends to zero, so that the oscillators end up being disconnected, in A_2 the link weight tends to one, which is not enough to synchronize the oscillators since $\sigma_c < \Delta$.

On the other hand, we have synchronization in regions $B_{1,2,3}$. B_1 is defined by $\Delta < \sigma_c < \Sigma_1$, with the critical curve Σ_1 defined in Eq. (A.3). B_2 is enclosed by $\sigma_c > \Sigma_1$ and $\sigma_c < \Sigma_2$, with Σ_2 defined in Eq. (A.4). Finally, B_3 is characterized by $\sigma_c > \Sigma_2$ and $p_c > 1/\sqrt{2}$. Whereas in B_1 the weight becomes one, in $B_{2,3}$ tends to $\Sigma_1/\sigma_c < 1$,

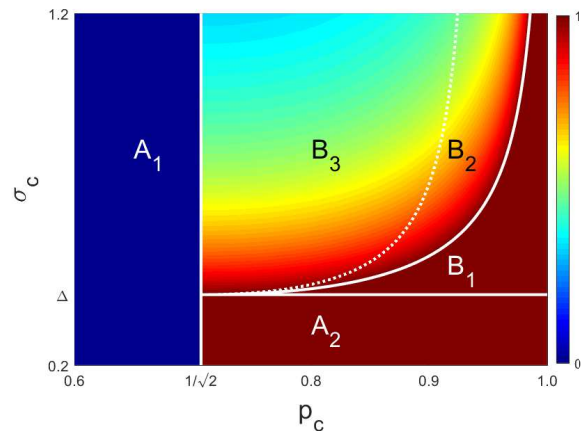


FIG. 5. Stability diagram for the link weight of a system of two coupled oscillators following Eqs. (5). The link weight tends to 0 in region A_1 and to 1 in region A_2 , but in both cases synchronization is impossible. Regions $B_{1,2,3}$ are characterised by phase locking: in B_1 the weight becomes one, whereas in $B_{2,3}$ the weight becomes $\Sigma_1/\sigma_c < 1$ with Σ_1 defined in Eq. (A.3). Regions B_2 and B_3 are different as the latter has a spiral sink, resulting in a slower convergence to the asymptotic state.

where Σ_1 is calculated in Eq. A.3. The difference between B_2 and B_3 is that we have a sink node in the first region and a spiral sink in the second one, which implies that the convergence in B_3 is slower than in B_2 .

Even for this simple two-node analysis, the scenario displayed by Fig. 5 fits closely the results obtained by numerical analysis for the evolution of large scale adaptive networks. This can be seen by comparison with Fig. 2(b), where the size of the giant component, which directly depends on the stationary weight values, was shown. In particular, the presence of the same structure in the parameter space allows us to consider that the analysis captures the relevant microscopic dynamics at the heart of the entanglement between structure and dynamics observed in the network resulting from the co-evolution process.

V. CONCLUSIONS

In conclusion, in this work we suggested a novel adaptive network model based on the competition between attractive coupling at the node level and anti-Hebbian repulsive dynamics at the link level. We showed how an initial set of fully interacting phase oscillators can naturally evolve towards a complex networked system, under the action of an adaptation mechanism which promotes interactions between elements that are not synchronized. Indeed, in many biological systems synchronization needs to be both promoted and controlled in order to avoid excessive redundancy. We characterized how the dynamical organization of the emerging systems leads sponta-

neously to degree-frequency correlation at the node level, a structure typically associated to networks able to sustain explosive synchronization. Our results can widen our understanding of the shaping mechanisms behind the structural organization of some real-world systems such as brain networks where the emergence of explosive synchronization has been observed. The stability analysis of a simplified model reveals the microscopic mechanisms that are at the heart of the observed emerging structural and dynamical features, and their non-trivial correlations, observed in the networks described by our adaptive coevolving model.

Appendix: Stability analysis

We compute the fixed points for Eq. (5), for which the following two cases need to be considered:

$$\begin{aligned} \phi^* &= \arcsin(\Delta/\sigma_c), \quad \alpha^* = 1; & (A.1) \\ \phi^* &= \arccos(2p_c^2 - 1), \quad \alpha^* = \frac{(\Delta/\sigma_c)}{2p_c\sqrt{1-p_c^2}}. & (A.2) \end{aligned}$$

As it is well known for the Kuramoto model, for ϕ to be locked it is required that $\sigma_c \geq \Delta$. Otherwise, neither ϕ^* in Eq. (A.1) nor α^* in Eq. (A.2) are well defined. Notice that Eq. (A.2) implies that $\alpha^* \geq \Delta/\sigma_c$, since $0 \leq p_c \leq 1$, and the weight α is constrained to be in the unit interval. This is a consequence of Eq. (2) that keeps all weights in the interval unit once the set of initial weights are chosen in that range.

The eigenvalues of the Jacobian matrix for Eq. (A.1) are

$$\lambda_1 = -\sigma_c \cos \phi^*, \quad \lambda_2 = \sqrt{\frac{1 + \cos \phi^*}{2}} - p_c.$$

Therefore, if $p_c < 1/\sqrt{2}$, we have a saddle point since $\lambda_1 < 0$ and $\lambda_2 > 0$. If $p_c > 1/\sqrt{2}$, there are two options

depending on the critical coupling strength

$$\Sigma_1 := \frac{\Delta}{2p_c\sqrt{1-p_c^2}}. \quad (A.3)$$

If $\sigma_c > \Sigma_1$, we again find a saddle point with $\lambda_1 < 0$ and $\lambda_2 > 0$, but if $\Delta < \sigma_c < \Sigma_1$, the fixed point is stable.

The corresponding Jacobian matrix for the second fixed point, Eq. (A.2), yields two more complex eigenvalues:

$$\lambda_{\pm} = \frac{A \pm \sqrt{A^2 + B(\frac{1}{\sigma_c} - \frac{1}{\Sigma_1})}}{C},$$

where $A := 2(1 - 2p_c^2)\Delta$, $B := 16p_c(1 - p_c^2)\Delta^2$ and $C := 8p_c\sqrt{1-p_c^2}$. Since B and C are always positive, we deduce that if $\sigma_c < \Sigma_1$, the fixed point is a saddle point with $\lambda_- < 0$ and $\lambda_+ > 0$. If $\sigma_c > \Sigma_1$, the stability depends on a second critical value Σ_2 that determines when the radicand becomes zero. This value can be defined as

$$\frac{1}{\Sigma_2} := \frac{1}{\Sigma_1} - \frac{(1 - 2p_c^2)^2}{4p_c(1 - p_c^2)}. \quad (A.4)$$

It can be verified easily that $\Sigma_2 > \Sigma_1$ for any value of Δ and p_c .

When $\Sigma_1 < \sigma_c < \Sigma_2$, we have either two positive eigenvalues, if $A > 0$ (i.e., if $p_c < 1/\sqrt{2}$), or two negative eigenvalues, if $A < 0$ (i.e., if $p_c > 1/\sqrt{2}$). On the other hand, if $\sigma_c > \Sigma_2$, the radicand is negative and, consequently, both eigenvalues are complex and the sign of the real part is given by the sign of A , positive for $p_c < 1/\sqrt{2}$ and negative for $p_c > 1/\sqrt{2}$.

ACKNOWLEDGMENTS

Work partly supported by SEP-PRODEP (Mexico) through the Project UACOH-PTC-322 DSA/103.5/15/7082. Work partly supported by the Spanish Ministry of Economy under projects FIS2013-41057-P and SAF2016-80240-P, and by GARECOM (Group of Research Excellence URJC-Banco de Santander). Authors acknowledge the computational resources and assistance provided by CRESCO, the supercomputing center of ENEA in Portici, Italy.

-
- [1] C. Zhou and J. Kurths, Physical Review Letters **96**, 2 (2006).
 - [2] P. De Lellis, M. Di Bernardo, and F. Garofalo, Chaos **18** (2008).
 - [3] S. Assenza, R. Gutiérrez, J. Gómez-Gardenes, V. Latora, and S. Boccaletti, Scientific reports **1**, 99 (2011).
 - [4] R. Gutiérrez, A. Amann, S. Assenza, J. Gómez-Gardenes, V. Latora, and S. Boccaletti, Phys. Rev. Lett.

107, 234103 (2011).

- [5] V. Avalos-Gaytán, J. A. Almendral, D. Papo, S. E. Schaeffer, and S. Boccaletti, Physical Review E **86**, 015101 (2012).
- [6] W. J. Yuan, J. F. Zhou, Q. Li, D. B. Chen, and Z. Wang, Physical Review E **88**, 1 (2013).
- [7] M. Chavez, M. Valencia, V. Navarro, V. Latora, and J. Martinerie, Physical review letters **104**, 118701 (2010).

- [8] K. P. Lamsa, J. H. Heeroma, P. Somogyi, D. A. Rusakov, and D. M. Kullmann, *Science* **315**, 1262 (2007).
- [9] E. Harvey-Girard, J. Lewis, and L. Maler, *Journal of Neuroscience* **30**, 6152 (2010).
- [10] D. E. Feldman, *Neuron* **75**, 556 (2012).
- [11] J. Myung, S. Hong, D. DeWoskin, E. De Schutter, D. B. Forger, and T. Takumi, *Proceedings of the National Academy of Sciences* **112**, E3920 (2015).
- [12] M. O. Magnasco, O. Piro, and G. A. Cecchi, *Physical review letters* **102**, 258102 (2009).
- [13] F. Scafuti and T. Aoki, **062913**, 1 (2015).
- [14] P. S. Skardal, D. Taylor, and J. G. Restrepo, *Physica D: Nonlinear Phenomena* **267**, 27 (2014).
- [15] V. K. Chandrasekar, J. H. Sheeba, B. Subash, M. Lakshmanan, and J. Kurths, *Physica D: Nonlinear Phenomena* **267**, 36 (2014).
- [16] J. Gómez-Gardeñes, S. Gómez, A. Arenas, and Y. Moreno, *Phys. Rev. Lett.* **106**, 128701 (2011).
- [17] I. Leyva, I. Sendina-Nadal, J. Almendral, A. Navas, M. Zanin, D. Papo, J. Buldú, and S. Boccaletti, *Scientific Reports* **3**, 1281 (2013).
- [18] I. Leyva, I. Sendina-Nadal, J. Almendral, A. Navas, S. Olmi, and S. Boccaletti, *Physical Review E* **88**, 042808 (2013).
- [19] A. Navas, J. Villacorta-Atienza, I. Leyva, J. Almendral, I. Sendina-Nadal, and S. Boccaletti, *Physical Review E* **92**, 062820 (2015).
- [20] S. Boccaletti, J. Almendral, S. Guan, I. Leyva, Z. Liu, I. Sendina-Nadal, Z. Wang, and Y. Zou, *Physics Reports* **660**, 1 (2016).
- [21] X. Zhang, S. Boccaletti, S. Guan, and Z. Liu, *Physical review letters* **114**, 038701 (2015).
- [22] A. E. Motter, S. A. Myers, M. Anghel, and T. Nishikawa, arXiv preprint arXiv:1302.1914 (2013).
- [23] I. Leyva, R. Sevilla-Escoboza, J. Buldú, I. Sendina-Nadal, J. Gómez-Gardeñes, A. Arenas, Y. Moreno, S. Gómez, R. Jaimes-Reátegui, and S. Boccaletti, *Physical review letters* **108**, 168702 (2012).
- [24] P. Kumar, D. K. Verma, P. Parmananda, and S. Boccaletti, *Physical Review E* **91**, 062909 (2015).
- [25] R. B. Yaffe, P. Borger, P. Megevand, D. M. Groppé, M. A. Kramer, C. J. Chu, S. Santaniello, C. Meisel, A. D. Mehta, and S. V. Sarma, *Clinical Neurophysiology* **126**, 227 (2015).
- [26] M. Kim, G. A. Mashour, S.-B. Moraes, G. Vanini, V. Tarnal, E. Janke, A. G. Hudetz, and U. Lee, *Frontiers in Computational Neuroscience* **10**, 1 (2016).
- [27] M. Kim, S. Kim, G. A. Mashour, and U. Lee, *Frontiers in Computational Neuroscience* **11**, 1 (2017).
- [28] Y. Kuramoto, “Chemical oscillations, waves and turbulence. 1984,”.
- [29] S. Boccaletti, J. Kurths, G. Osipov, D. Valladares, and C. Zhou, *Physics reports* **366**, 1 (2002).
- [30] V. Nicosia, M. Valencia, M. Chavez, A. Díaz-Guilera, and V. Latora, *Physical review letters* **110**, 174102 (2013).
- [31] V. A. Maksimenko, A. Lüttjohann, V. V. Makarov, M. V. Goremyko, A. A. Koronovskii, V. Nedaivozov, A. E. Runnova, G. van Luijtelaa, A. E. Hramov, and S. Boccaletti, *Physical Review E* **96**, 012316 (2017).
- [32] J. A. Acebrón, L. L. Bonilla, C. J. P. Vicente, F. Ritort, and R. Spigler, *Reviews of modern physics* **77**, 137 (2005).